Some influences of stratigraphy and structure on reservoir stress orientation

Michael S. Bruno* and Don F. Winterstein‡

ABSTRACT

The azimuth of maximum horizontal stress in a reservoir can vary significantly with depth and with position on a subsurface structure. We present and discuss evidence from field data for such variation and demonstrate both analytically and with finite-element modeling how such changes might take place. Under boundary conditions of uniform far-field displacement, changes in stratigraphic layering can reorient the principal stress direction if the formation is intrinsically anisotropic. If the formation stiffness is lower perpendicular to bedding than parallel to bedding (as is often the case in layered geologic media), an increase in dip will reduce the component of compressive stress in the dip azimuth direction. Folds can reorient principal stresses because flexural strain varies with depth and position. Compressive stress perpendicular to a fold axis increases with depth at the crest of an anticline and decreases with depth at the limb. When the regional stress anisotropy is weak, this change in stress magnitude can reorient the local principal stress directions. Numerical simulations of such effects gave results consistent with changes in stress orientation at the Cymric and Lost Hills oil fields in California as observed via shear-wave polarization analyses and tiltmeter surveys of hydraulic fracturing. Knowledge of such variation of stress direction with depth and structural position is critical for drilling, completions, hydraulic fracture, and well pattern designs.

INTRODUCTION

The orientation of in-situ stresses strongly influences several reservoir characteristics related to drilling, stimulation, and production. During drilling operations, for example, the magnitudes and orientations of stresses determine mud-weight limits required to avoid wellbore collapse or unintentional fracture and lost circulation. Stress orientation is especially important in the design of horizontal completions because wellbore stability and propensity to fracture vary with well inclination and azimuth. During production, stress-induced near-wellbore damage can cause sanding problems. In naturally or hydraulically fractured reservoirs, effective fracture widths, fluid conductivity, and fracture orientation are directly related to stress direction and magnitude. The resulting permeability anisotropy must be considered when developing dense well spacing designs and line-drive waterflood operations.

In many reservoirs, the direction of maximum stress can vary significantly with both depth and structural location. This is especially true in reservoirs that are structurally complex, as in the Rocky Mountain region or in tectonically active regions such as California. Variations in stress orientation are often related to changes in lithology and structure and can arise from the inherent anisotropy of geologic materials. While it is common practice to account for reservoir stress *magnitude* changes with depth and sometimes location throughout a field, relatively little recognition is given to the variations in reservoir stress *orientation* and the important implications these variations may have on development strategies.

A common practice has been to explain stress anisotropy by imposing a far-field (tectonic) deviatoric *stress* boundary condition on the reservoir. But numerous field observations reveal that stress magnitudes vary across lithologic boundaries. Hence it is more appropriate to impose tectonic *strain* or far-field displacement boundary conditions. It then becomes apparent that changes in stratigraphic layering, dip, lateral heterogeneity, and local structure may reorient the principal stress directions.

The purpose of this paper is to describe some influences of stratigraphy and structure on stress orientation, and to present analytical and numerical techniques to estimate changes with depth and structural position. We first review field evidence for variations in maximum horizontal stress direction with depth and position around reservoirs followed

Manuscript received by the Editor December 14, 1992; revised manuscript received November 8, 1993.
*Terralog Technologies, 332 E. Foothill Blvd., Arcadia, CA 91006.
‡Chevron Petroleum Technology Co., P.O. Box 446, La Habra, CA 90633-0446.

by a brief description of stress-strain relations for anisotropic rocks. We then describe analytically some stratigraphic influences on stress orientation and illustrate them with a numerical example of stress reorientation caused by changing dip across an unconformity, given a uniform far-field displacement boundary condition. Next, we illustrate some structural influences with an example of stress variations within anticlinal structures. We include field observations consistent with each of these situations.

FIELD OBSERVATIONS OF STRESS DIRECTION CHANGES

A common early practice was to express horizontal stress as a linear function of depth, dependent on overburden density and a constant Poisson's ratio. It is now recognized that horizontal stresses in a reservoir are not related solely to depth but depend strongly on lithology, burial history, bedding, faults, and sometimes surface topography (Zoback et al., 1980; Warpinski et al., 1985; Evans and Engelder, 1986). In the Piceance Basin, Colorado, horizontal stresses are anisotropic in sandstone formations and nearly isotropic in bounding shale formations (Teufel, 1986). Fault related variations in shear stress and principal stress orientation have been noted near the San Andreas fault in Mojave desert wells (Hickman et al., 1988) and in the Cajon Pass Scientific Drillhole (Shamir and Zoback, 1992). Bedding and topography appear to reorient stress by as much as 45 degrees at Ranier Mesa at the Nevada Test Site (Warpinski and Teufel, 1991).

Several field techniques may be used to determine the directions of principal in-situ stresses. Three common techniques use borehole breakouts (Gough and Bell, 1982; Zoback et al., 1985), hydraulic fracture traces in open-hole sections (Smith et al., 1986), and surface tilt during hydraulic fracture operations (Davis, 1983; Evans, 1983). A more recently developed technique is polarization analysis of vertically traveling shear waves (*S*-waves) in birefringent rocks (Winterstein and Meadows, 1991a and b). Figure 1 shows data from the Cymric oil field in California, where the direction of maximum horizontal stress is believed to lie along the polarization direction of the fast *S*-wave. A dramatic shift occurs near the angular (Plio-Miocene) unconformity, across which the stratigraphic dip changes by about 35 degrees.

The direction of maximum stress in a reservoir varies not only with depth and lithology but sometimes also with structural position. For example, Figure 2 shows the maximum horizontal stress directions in the Ekofisk Field determined by Teufel and Farrell (1992) with microfracturing techniques. Maximum stress is generally perpendicular to the structural contour lines. Radial faulting associated with this type of stress pattern is common above salt diapirs and other piercement domes (Withjack and Scheiner, 1982).

Several published reports have described variations in fracture patterns across fold-related structures (Price, 1966; Stearns, 1968). While it is intuitive that these fracture patterns may indicate variations in stress direction, very few field studies have been conducted to quantify changes in stress orientation across structures. The results of one such study conducted recently by Chevron are presented in Figure 3, which shows the variation in fast shear-wave polarization angles across the Lost Hills Field in California.

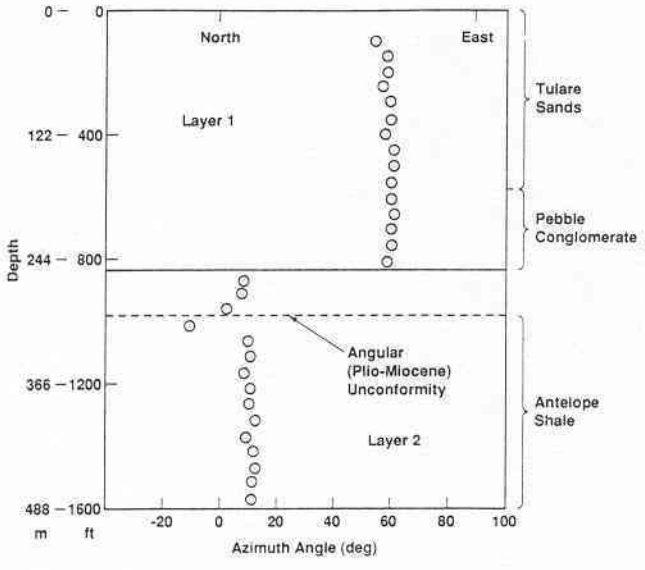

FIG. 1. Polarization angles of the fast *S*-wave in Cymric Field. Maximum horizontal stress directions are believed to lie along these polarization directions.

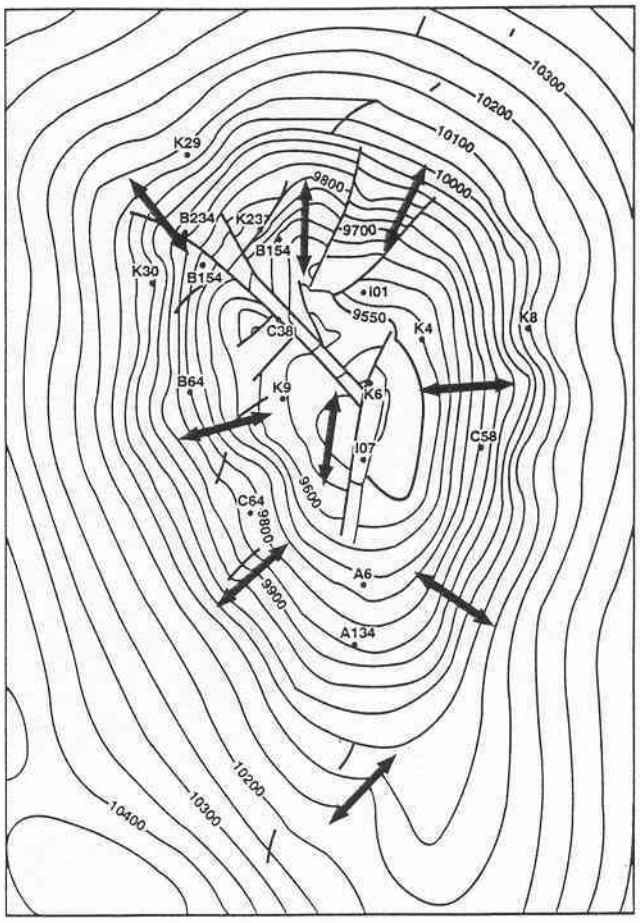

FIG. 2. Maximum horizontal stress directions in the Ekofisk Field are generally perpendicular to the structural contours. Reprinted with permission from Teufel and Farrell (1992).

[Results from Well 1-9J are in Winterstein and Meadows, (1991a).] The direction of maximum compressive horizontal stress inferred is more northerly near the crest of the anticline and rotates toward a direction nearly perpendicular to structural contour lines at the reservoir flanks. For comparison, structural contours and faulting patterns are presented in Figure 4.

The general trends in shear-wave analysis results at Lost Hills are consistent with trends from hydraulic fracture tiltmeter measurements (Figure 5) and with the pattern of normal faulting across the field (Figure 4). In addition to variation in principal stress direction with lateral position, field measurements also indicate that the principal stress direction rotates with depth at Lost Hills. Interestingly, although data are limited, the rotation as a function of depth that occurs near the crest of the anticline tends to be opposite in sense to the rotation that occurs near the flanks. Basic deformation and mechanics principles for folded structures, described later, provide a possible explanation for this behavior.

The next two sections in this paper present the analytical background for modeling stress-strain behavior in geologic materials and for evaluating ways in which changing stratigraphy and structural position can reorient maximum stress directions.

STRESS-STRAIN BEHAVIOR FOR ANISOTROPIC ROCKS

Stress at a point in a solid is defined by the net force per unit area (traction vector) acting on each of three orthogonal planes through that point. Consider a small volume element in a Cartesian coordinate system (x, y, z) as shown in Figure 6. The force vectors may be resolved into normal and shear components and divided by the surface area on each face to define the nine components of the stress tensor σ_{ij}, where the subscripts indicate stress on the ith face acting in the jth direction. (The tensor indices i and j can take on any value x, y, or z). Compressive stresses and strains will be defined as positive.

For many reservoirs, the far-field stress state is controlled by a regional tectonic displacement field. The strain tensor ε_{ij} is defined by the gradients of this displacement field. Extensional or compressional deformations associated with length and volume changes are defined by the normal strain components ε_{xx}, ε_{yy}, and ε_{zz}. Angular distortions are defined by the shear strain components ε_{xy}, ε_{xz}, and ε_{yz}. Stress and strain are symmetric tensors and may be represented in full matrix notation by the following relations:

$$\sigma_{ij} \Rightarrow \begin{bmatrix} \sigma_{xx} & \sigma_{xy} & \sigma_{xz} \\ \sigma_{xy} & \sigma_{yy} & \sigma_{yz} \\ \sigma_{xz} & \sigma_{yz} & \sigma_{zz} \end{bmatrix}, \tag{1}$$

$$\varepsilon_{ij} \Rightarrow \begin{bmatrix} \varepsilon_{xx} & \varepsilon_{xy} & \varepsilon_{xz} \\ \varepsilon_{xy} & \varepsilon_{yy} & \varepsilon_{yz} \\ \varepsilon_{xz} & \varepsilon_{yz} & \varepsilon_{zz} \end{bmatrix}. \tag{2}$$

Stresses are related to strains through the mechanical properties of the material. A common engineering procedure is to assume that the ideal rock mass is linearly elastic, isotropic, continuous, and homogeneous. However, real rocks are nonideal in several ways. They are seldom continuous at any scale because they contain pores, microfractures, joints and faults, and stratigraphic layers of varying lithology. These features modify stresses and often impart directionality, or *anisotropy*, to the material. The material anisotropy, whether inherent or stress induced, strongly influences the local stress orientation.

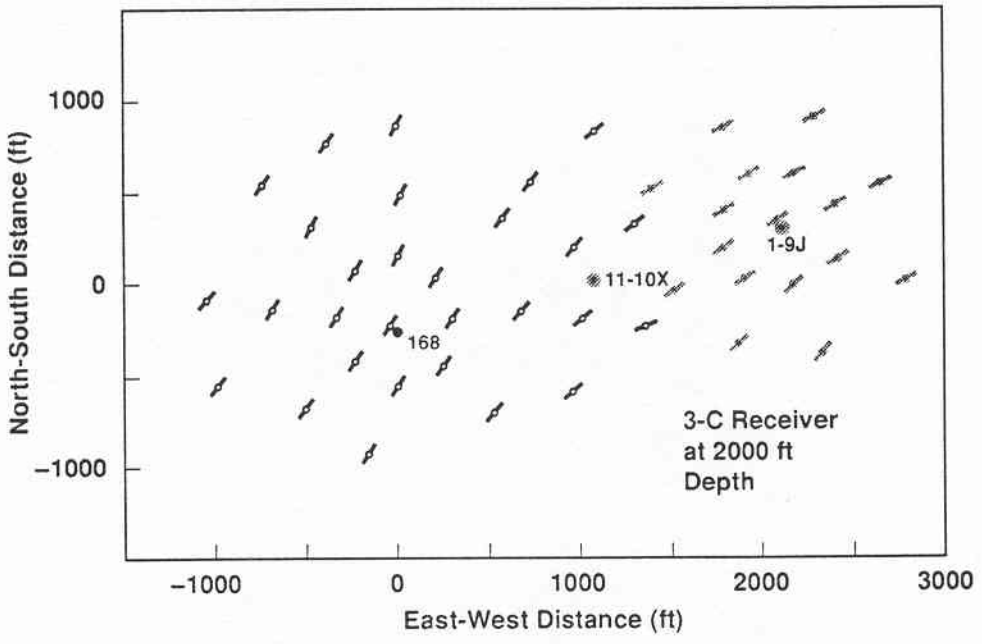

FIG. 3. Fast S-wave polarization directions in Lost Hills Field. Systematic change from Well 168 to Well 1-9J probably indicates a corresponding change in the direction of maximum horizontal compressive stress. The dark lines with open circles are from analysis of Well 168 data and the light lines with solid circles are from Well 1-9J. For both data sets a 3-component geophone was clamped at a depth of 2000 ft (610 m) while the seismic source was activated at locations represented by the centers of the line segments.

For linear elastic deformation of anisotropic materials, stresses are related to strains through stiffness coefficients $C_{ijk\ell}$. In tensor notation (with repeated indices signifying summation) the constitutive equations are

$$\sigma_{ij} = C_{ijk\ell}\varepsilon_{k\ell}. \tag{3}$$

Equation (3) is valid only over the range for which the coefficients $C_{ijk\ell}$ remain constant, where stress and strain changes are small.

Because there are nine stress tensor components related to nine strain tensor components, the most general form of equation (3) would contain 81 stiffness coefficients. However, not all of them are independent, and some are identically zero. Symmetry of both stress and strain tensors, combined with strain energy considerations, reduces the number of independent stiffness coefficients to 21. Finally, the consideration of pure mode directions (Winterstein, 1990) reduces the maximum number of independent coefficients for an anisotropic material with no symmetry planes to 18 (Fedorov, 1968). Because of depositional history, geologic materials will generally contain a plane of material symmetry aligned with the bedding that further reduces the

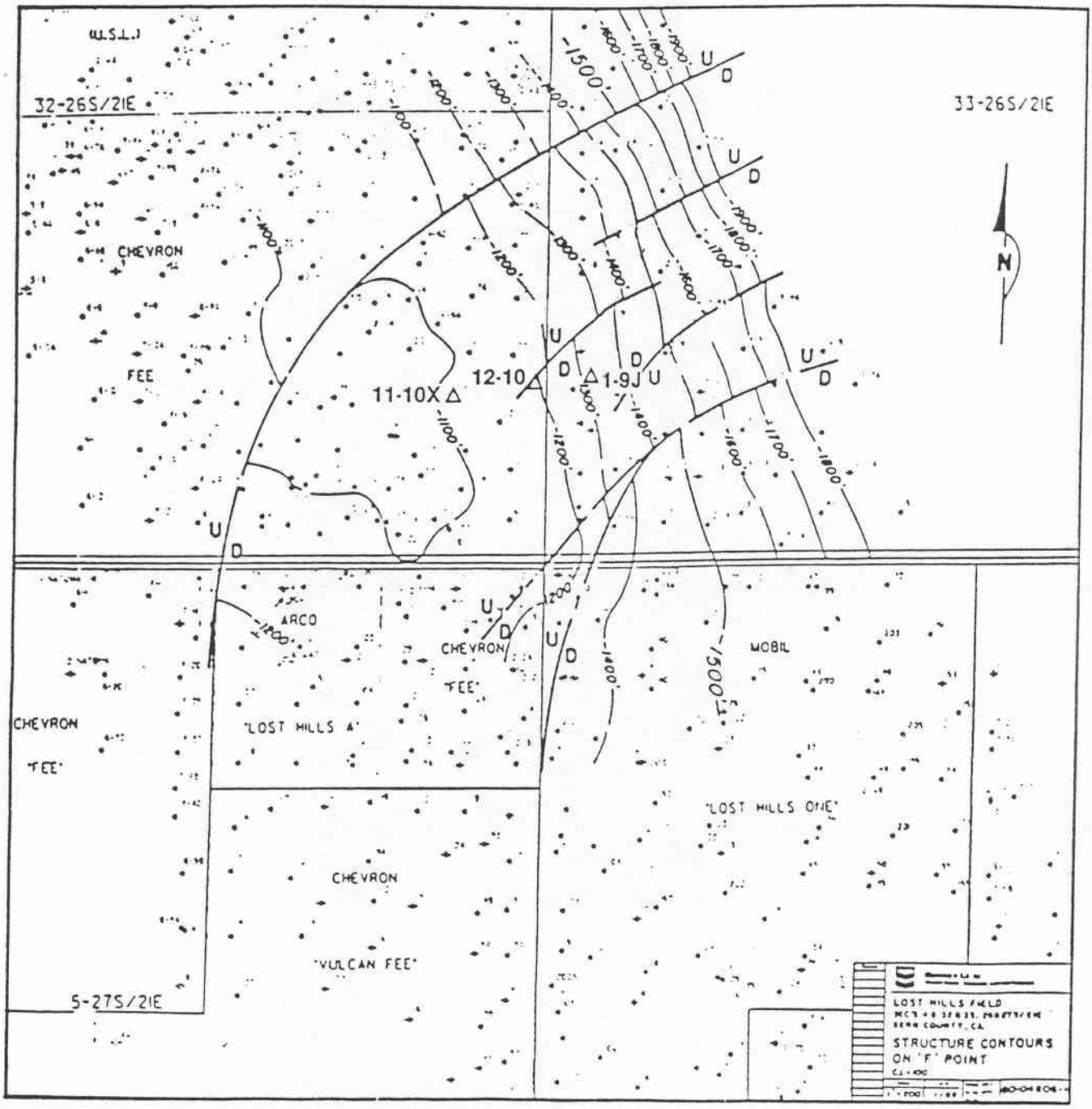

FIG. 4. The direction of normal faults in the Lost Hills Field rotates from the axis of the structure towards the flank.

number of independent stiffness coefficients. Although dipping fracture sets or multiple vertical sets can induce anisotropy of low symmetry, for most purposes we assume geologic formations contain three orthogonal planes of material symmetry, and are thus *orthotropic* or *orthorhombic*. The elastic properties of an orthotropic material can be described completely with nine independent stiffness coefficients. For materials of such symmetry, a contracted matrix form of tensor equation (3) may be expressed as

$$\begin{Bmatrix} \sigma_{xx} \\ \sigma_{yy} \\ \sigma_{zz} \\ \sigma_{yz} \\ \sigma_{xz} \\ \sigma_{xy} \end{Bmatrix} = \begin{bmatrix} C_{xxxx} & C_{xxyy} & C_{xxzz} & & & \\ C_{xxyy} & C_{yyyy} & C_{yyzz} & & & \\ C_{xxzz} & C_{yyzz} & C_{zzzz} & & & \\ & & & C_{yzyz} & & \\ & & & & C_{xzxz} & \\ & & & & & C_{xyxy} \end{bmatrix} \times \begin{Bmatrix} \varepsilon_{xx} \\ \varepsilon_{yy} \\ \varepsilon_{zz} \\ 2\varepsilon_{yz} \\ 2\varepsilon_{xz} \\ 2\varepsilon_{xy} \end{Bmatrix}. \quad (4)$$

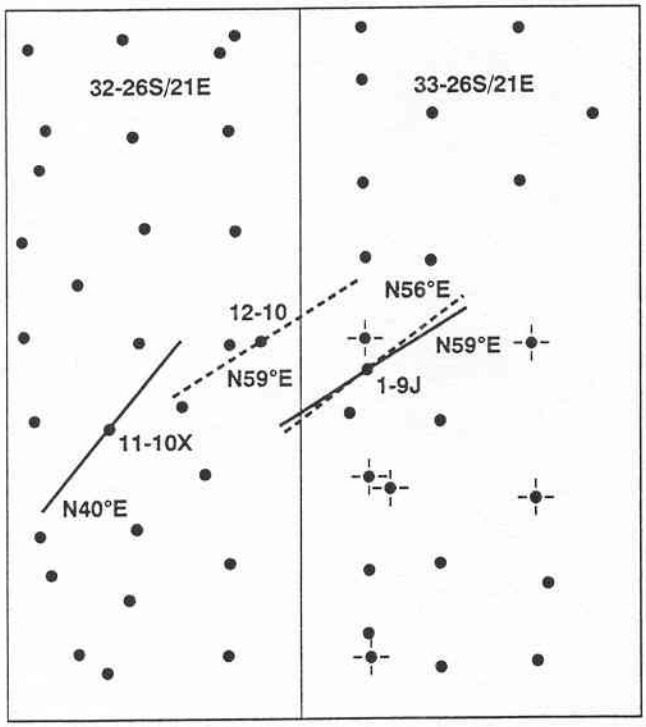

FIG. 5. Fast *S*-wave polarization directions (solid) compare well with hydraulic fracture orientations determined by tiltmeter surveys (dashed) in the Lost Hills field.

A popular alternate notation places single subscripts on stresses and strains and double subscripts on the stiffness coefficients (Winterstein, 1990).

Orthorhombic materials include, for example, layered geologic formations with a single dominant fracture set oriented perpendicular to the bedding plane. Layering without oriented fractures will produce geologic formations that are *transversely isotropic*, or isotropic in all directions parallel to bedding. For these materials $C_{xxxx} = C_{yyyy}$, $C_{xxzz} = C_{yyzz}$, $C_{yzyz} = C_{xzxz}$, and $2C_{xyxy} = C_{xxxx} - C_{xxyy}$. All other constants are zero, so only five are independent. Finally, completely isotropic materials may be described with only two independent constants. The stiffness coefficients in equation (4) expressed in terms of related engineering properties and wave velocities for the isotropic case are given by

$$C_{xxxx} = C_{yyyy} = C_{zzzz} = \frac{E(1-v)}{(1+v)(1-2v)} = \lambda + 2\mu = \rho V_p^2 \quad (5)$$

$$C_{yzyz} = C_{xzxz} = C_{xyxy} = \frac{E}{2(1+v)} = \mu = \rho V_s^2 \quad (6)$$

$$C_{xxyy} = C_{xxzz} = C_{yyzz} = \frac{Ev}{(1+v)(1-2v)} = \lambda = \rho V_p^2 - 2\rho V_s^2, \quad (7)$$

where E is Young's Modulus, v is Poisson's ratio, λ and μ are the Lamé constants, ρ is density, V_p is compressional wave speed, and V_s is the shear-wave speed for the formation material.

At any point in a reservoir there is a unique set of orthogonal directions in which all stresses are normal (principal). The principal stress directions are given by the eigenvectors of σ_{ij}, and the largest magnitude is equal to the largest eigenvalue. Similarly, there is a unique set of orthog-

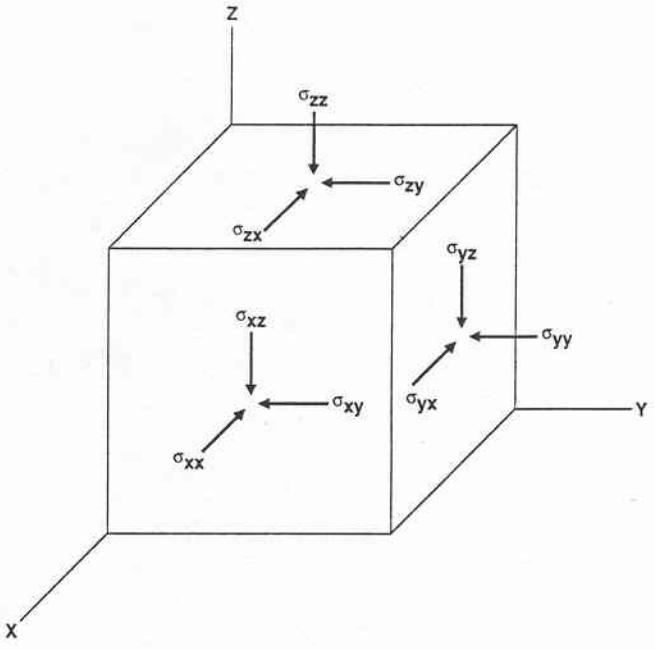

FIG. 6. Stresses acting on a volume element.

onal directions in which only normal strains occur, defined by the eigenvectors of ε_{ij}. For anisotropic materials the directions of principal stress do not necessarily coincide with the directions of principal strain, as they must for isotropic materials. The practice of decomposing stress-strain relations into volumetric and deviatoric components, which is common for isotropic materials, is no longer meaningful. Purely normal stresses can induce shear strains. Pure extension or compression can induce shear stresses and hence a rotation in the direction of principal stress with respect to the direction of principal strain. The key point is that, even if the regional deformation field acting on a reservoir is uniform, variations in principal stress direction can easily occur because of changes in material properties.

In the absence of additional loading (including thermal or fluid pressure changes) there are two ways that the local state of stress within a reservoir may vary with depth or location. Either the material properties can change or the local strain tensor can change [see equation (3)]. A change in lithology or change in amount or orientation of fracturing can result in modified material properties. In the absence of bedding plane slip, strain fields are continuous across lithologic boundaries, but some of the stress components are not. For anisotropic materials the eigenvectors of the modified stress field are generally different from the eigenvectors of the original stress field, and hence the direction of maximum stress changes. For a given uniform strain field, the direction of maximum stress will remain unchanged only if the material axes both above and below the lithology boundary are aligned with each other. Material axes here are symmetry axes of orthorhombic or transversely isotropic materials.

If the lithology does not vary, a change in bedding dip across a stratigraphic boundary can also modify the stress field in anisotropic materials because the material axes may not match across the boundary. Modification of the stiffness coefficients can be expressed through the tensor transformation,

$$C_{ijk\ell} = a_{im} a_{jn} a_{kp} a_{\ell r} C'_{mnpr}, \tag{8}$$

where the direction cosines are given by $a_{ij} = \cos(\theta)$, and θ is the angle between the reference coordinate axis x_i and a rotated material coordinate axis x'_j. Such changes and their potential influence on principal stress direction can sometimes be inferred from dipmeter logs.

The direction of maximum stress can also vary in a formation simply as a result of a modification in the local strain tensor, even in isotropic materials. This situation may occur, for example, above and below the neutral surface of an anticline, which separates an area of layer-parallel compression from layer-parallel extension. Abrupt changes in strain magnitude or orientation may also occur across opposite sides of a fault. In such situations, the azimuth of maximum stress will remain unchanged only if the orientation of the structural axis or the fault plane is aligned with a regional principal stress direction. Analytical and numerical examples are presented in the following two sections to illustrate some of these stratigraphic and structural influences on stress orientation.

STRATIGRAPHIC INFLUENCE ON STRESS ORIENTATION

Consider a layered geologic medium in which the formations undergo an abrupt change in dip. This can occur, for example, when younger flat lying beds are deposited on beds that have been tilted, uplifted, and eroded. Figure 7 is a schematic representation of such an example where the material axes of the lower section are rotated relative to those of the upper section. Define a coordinate system (x, y, z) aligned with the upper stratigraphic units and a rotated coordinate system (x', y', z') aligned with the lower stratigraphic units, as shown in Figure 7. Consider the situation in which the lower stratigraphic units are rotated clockwise through an azimuthal angle θ_a about the z-axis and downward through a dip angle θ_d about the y'-axis. Let both the upper and lower units be composed of identical transversely isotropic materials with symmetry axes perpendicular to bedding.

The direction cosines relating the stiffness coefficients of the rotated material in the lower section to those of the unrotated material in the upper section are:

$$\begin{aligned}
a_{xx'} &= \cos(\theta_a)\cos(\theta_d),\\
a_{yy'} &= \cos(\theta_a),\\
a_{zz'} &= \cos(\theta_d),\\
a_{xy'} &= \cos(\theta_a + 90) = -\sin(\theta_a),\\
a_{yx'} &= \cos(90 - \theta_a)\cos(\theta_d) = \sin(\theta_a)\cos(\theta_d),\\
a_{zx'} &= \cos(90 + \theta_d) = -\sin(\theta_d),\\
a_{xz'} &= \cos(\theta_a)\cos(90 - \theta_d) = \cos(\theta_a)\sin(\theta_d),\\
a_{yz'} &= \cos(90 - \theta_a)\cos(90 - \theta_d)\\
&= \sin(\theta_a)\sin(\theta_d), \quad \text{and}\\
a_{zy'} &= 0.
\end{aligned} \tag{9}$$

For a given strain field and given material properties, equations (3), (8), and (9) may be used to estimate analytically what influence a change in stratigraphic dip might have on the direction of maximum stress. [Alternatively, using the vector/matrix notation, one can calculate the new stiffness

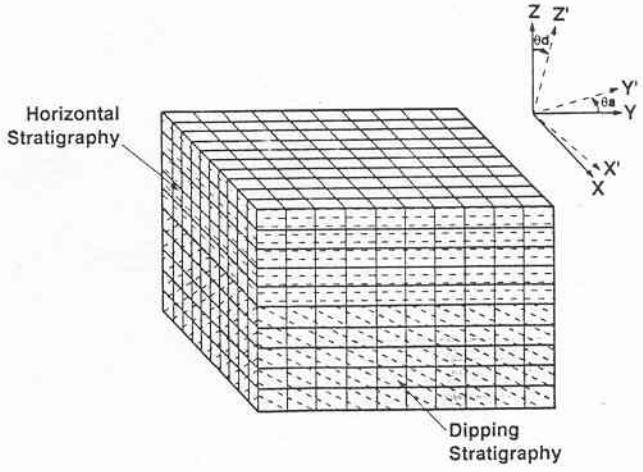

FIG. 7. Dipping lithology schematic and finite-element model. Element θ_d is the dip angle from vertical and θ_a is the dip azimuth.

coefficients and stress components by means of Bond transformations (Winterstein, 1990)]. To illustrate, we consider two transversely isotropic materials, both with stiffnesses given in Table 1. When the strain field is held fixed, the direction of principal stress rotates in the dipping material relative to that in the flat lying material. Table 2 gives the angle by which the horizontal component of the maximum principal stress rotates as a function of the lower layer azimuthal orientation and dip angles, θ_a and θ_d. The example presented is for a compressive far-field strain of $\varepsilon_{xx} = 0.011$ and $\varepsilon_{yy} = 0.010$, taken to be identical for both layers.

The material properties for this example (Table 1) were chosen in part to give a rotation of horizontal principal stress in the positive sense for the given far-field strain and the given dip and azimuthal orientation angles (Table 2). In this context, "positive" implies a rotation in the northerly direction from an initially northeasterly direction, the sense of rotation observed in the Cymric data of Figure 1. To get this sense of rotation from transversely isotropic materials requires the stiffness perpendicular to bedding to be higher than that parallel to bedding. Such a configuration is not common in sedimentary rocks but could originate from a set of vertical fractures with randomly oriented azimuths. The actual rocks at Cymric and other places, where vertical *S*-wave birefringence is large, are likely to be orthorhombic, and suitable orthorhombic properties would produce the sense of rotation observed.

Besides the analytical approach just illustrated, we can also use finite-element techniques to investigate effects of changing stratigraphy on stress direction. The model shown in Figure 7 was discretized into 1000 blocks for analysis with the ADINA finite element program (ADINA R&D Report ARD 87-1, 1987) in an effort to simulate the Cymric oil field. The maximum compression direction was taken to be N60°E, roughly perpendicular to the nearby San Andreas fault. Because detailed rock properties were not available, and our intention was to compare stress rotation only qualitatively, we modeled both the upper flat lying Tulare sands and conglomerate and the southwest dipping Antelope shale units with the transversely isotropic stiffnesses in Table 1.

Stress rotations from both the finite-element model and the analytical technique are shown in Figure 8. A comparison with the field data in Figure 1 shows that the dipping stratigraphy may account for much of the observed northerly shift in maximum horizontal stress across the unconformity. The shift direction is consistent, but the magnitude of shift indicated in the *S*-wave data (about 45 degrees) is larger than that of the numerical model (about 30 degrees). Although something other than changing dip, such as oriented fractures or residual paleostress, could be responsible for the observed stress rotation, the exercise demonstrates that a rather simple analysis of stratigraphy predicts a rotation of maximum horizontal stress similar to that observed.

Table 1. Normalized stiffness coefficients for dipping lithology example (MPa).

$C_{xxxx} = 1.25$	$C_{xxyy} = 0.45$	$C_{yzyz} = 0.45$
$C_{yyyy} = 1.25$	$C_{xxzz} = 0.55$	$C_{xzxz} = 0.45$
$C_{zzzz} = 1.66$	$C_{yyzz} = 0.55$	$C_{xyxy} = 0.40$

Table 2. Direction of the horizontal component of the maximum principal stress in the dipping layer, expressed in degrees from the *x*-axis, for several dip and azimuthal orientation angles.

	Azimuthal orientation angle, θ_a			
Dip, θ_d	0	15	30	45
0	0	0	0	0
15	0	4.7	9.0	12.4
30	0	9.1	18.6	28.7
45	0	11.1	22.6	35.1

INFLUENCE OF FOLDS ON STRESS ORIENTATION

Stress variations within folded structures have been studied analytically (Biot, 1964), numerically (Dieterich and Onat, 1969), and in the field, primarily through observations of rock fabric changes (Dieterich and Carter, 1969; Carter and Raleigh, 1969). The field studies generally indicate that the maximum compressive stress is inclined at small angles to the dip and perpendicular to strike along the fold limbs (Dieterich and Carter, 1969; Carter and Friedman, 1965). For folds formed by compression, the stress and strain depend on the material heterogeneity and amount of slip between bedding layers. Folds in which the bedding layers are nearly homogeneous and deform with little relative slip are *tangential longitudinal strain folds*. Those that develop significant

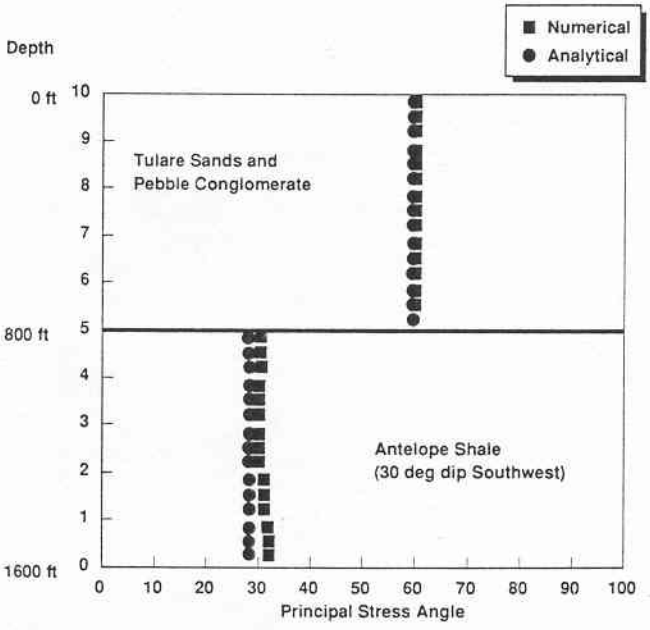

FIG. 8. The direction of maximum horizontal stress across the angular unconformity at the Cymric field was determined both analytically and with the finite-element model shown in Figure 7. Material stiffnesses above and below the unconformity were identical (Table 1). The change in stress azimuth resulted solely from differences of dip under the constraint of uniform far-field displacement.

relative slip between individual layers are *flexural slip folds*. The locations of maximum horizontal compressional stresses perpendicular to the fold axis are indicated in Figure 9 for these two situations. Flexural slip folds tend to influence local stress direction less strongly than tangential longitudinal strain folds.

When the regional stress anisotropy is small, the local stress concentrations can reorient principal stress directions. This is because the compressional stress perpendicular to the fold axis (shaded portions in Figure 9) varies with position as a result of the flexural strain in the fold. For example, when moving uphole at the crest of an anticline of the type shown in Figure 9b, compressive stress perpendicular to the fold axis decreases and the direction of maximum horizontal stress tends to rotate into a direction more parallel to the fold axis. Moving uphole at the limb of an anticline would tend to rotate the maximum horizontal stress more normal to the fold axis (perpendicular to structural strike). Moving laterally from the crest toward the flank of a reservoir, the maximum horizontal stress would also tend to rotate into a direction normal to the structural strike.

Such structural influences on principal stress directions may account for the rotation observed in the Lost Hills Field, as illustrated in Figures 3, 4, and 5. Tiltmeter surveys for hydraulic fracture azimuths at Lost Hills also reveal a sense of rotation with depth, about 10 degrees in a northerly direction moving uphole at the crest and about 7 degrees in an easterly direction moving uphole at the flank, trends consistent with the expected structural influence on stress direction. It should be noted, however, that other explanations for the stress rotation within the formation are possible, such as a rotation in regional stress or rotation of the structural axis over geologic time.

A finite-element model such as that in Figure 10 may be applied to analyze principal stress direction changes with depth and position within single layer or multilayered folded structures. For example, Figure 11 presents the rotation of maximum horizontal stress with depth for an anticline modeled with a stiff single layer embedded in a softer formation, given a far-field deformation of $\varepsilon_{xx} = 0.01$, $\varepsilon_{yy} = 0.02$, and $\varepsilon_{xy} = 0.01$. The contrast in Young's modulus between the stiff and soft formation is 10:1. A comparison is provided of the stress rotation at the crest and limb of the anticline. Stresses at the crest (Figure 11, left) of the anticline rotate uphole about 25 degrees toward a direction more parallel to the fold axis (oriented 0 degrees from x-axis). Stresses at the limb (Figure 11, right) of the structure rotate uphole towards a direction more normal to the fold axis.

Figure 12 shows the rotation of maximum horizontal stress with depth for an anticline modeled with three stiff layers, each of which is bounded by thin layers of soft material (Figure 10). The far-field strain and the modulus contrast are

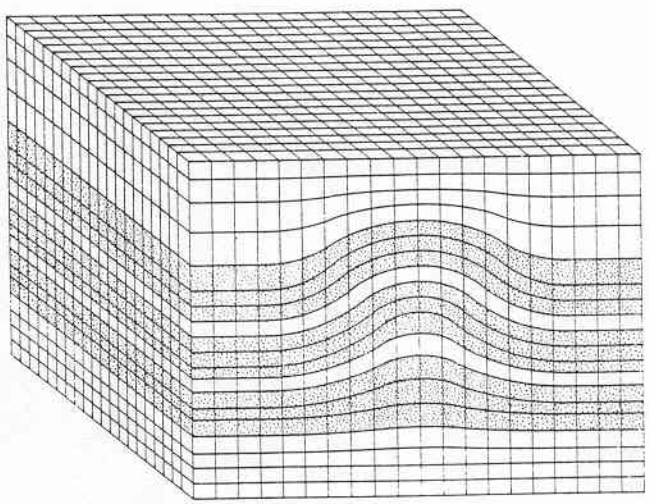

FIG. 10. A multilayered finite-element model may be used to simulate stress variations in anticlinal structures.

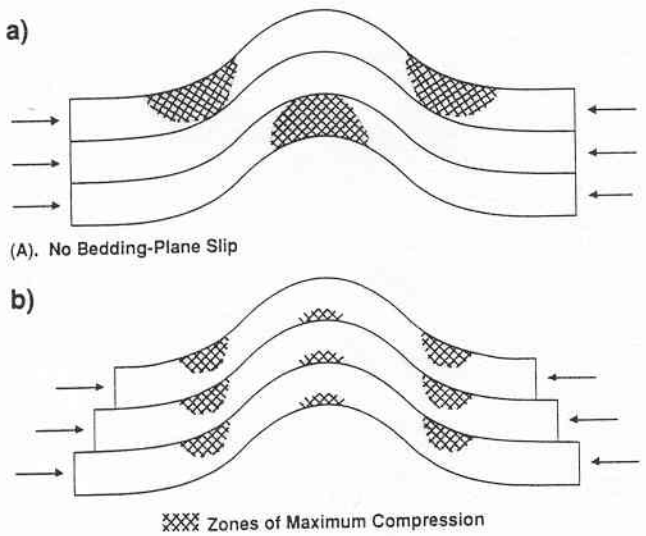

FIG. 9. Stress variations within folds. (a) No bedding-plane slip and (b) with bedding-plane slip. Shading indicates concentrations of compressive stress perpendicular to the fold axes.

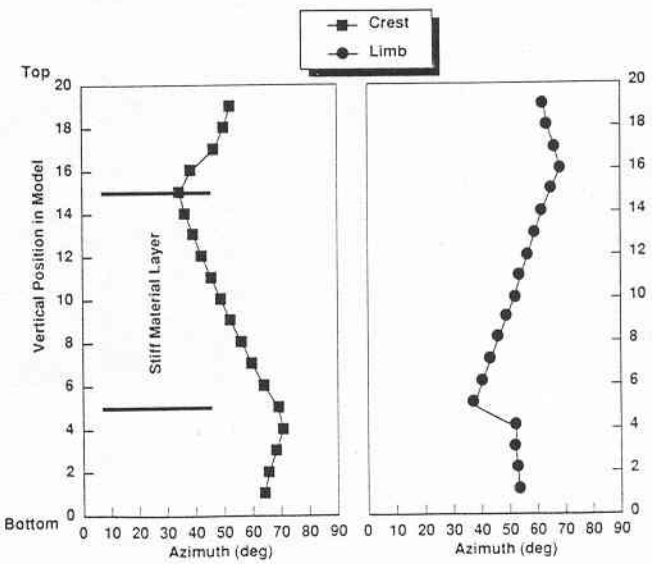

FIG. 11. Rotation of principal stress in an anticline with a single stiff layer. Fold axis is at zero degrees. Heavy lines indicate boundaries with softer material.

identical to those of the single-layer example. The stress rotation in each layer is similar in sense to that of the single-layer fold but of lower magnitude. Additional large variations in stress direction occur at the interbedded soft layers, demonstrating that material heterogeneity and structure can act in combination to influence stress in some formations. The anomalous variation in S-wave polarization direction from 900 to 1200 ft (274–366 m) in the Lost Hills Well 1-9J (Winterstein and Meadows, 1991a) may be related to a soft layer effect, as that zone was shalier than the rest of the section.

CONCLUSIONS

This paper presents field observations, analytical solutions, and numerical model results to illustrate that the direction of maximum horizontal stress within a reservoir can vary with depth and with position on a subsurface structure. Since principal stress orientation may be critical to some drilling, stimulation, and production operations, simple assumptions of constant stress orientation should be avoided. Stress orientation measurements at several locations within a formation are generally recommended. While it is difficult to estimate far-field boundary conditions and material properties within a reservoir, analytical and numerical models can sometimes be used with regional deformation and stress data to provide a qualitative estimate of stratigraphic and structural influences on local stress orientation within a reservoir. These estimates may then be confirmed or modified with field measurements at a few key locations.

ACKNOWLEDGMENTS

Mark Meadows, Dan Szymanski, and Dale Julander provided valuable support in acquiring and interpreting some of the field data. We also thank Chevron Oil Field Research Company and Chevron USA for supporting this investigation and for permission to publish the results.

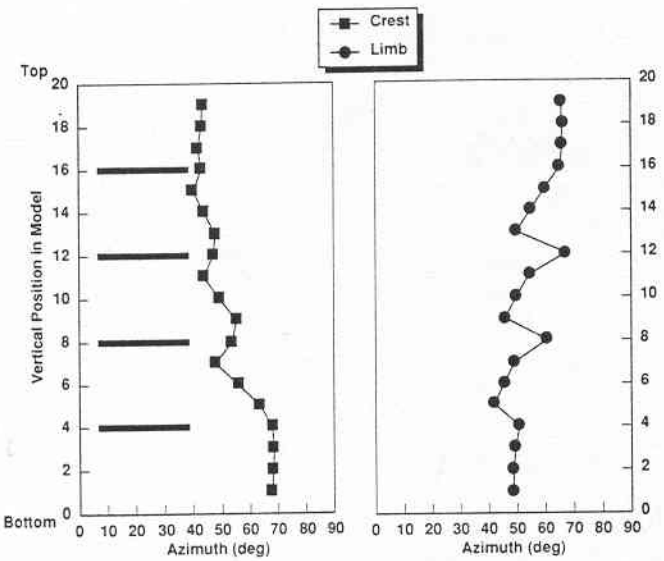

FIG. 12. Rotation of principal stress in multilayer anticline. Heavy lines indicate soft material layers.

REFERENCES

Biot, M. A., 1964, Theory of viscous buckling and gravity instability of multilayers with large deformation: Geol. Soc. Am. Bull., **76**, 371–378.

Carter, N. L., and Friedman, M., 1965, Dynamic analysis of deformed quartz and calcite from the Dry Creek Ridge Anticline, Montana: Am. J. Sci., **263**, 747–785.

Carter, N. L., and Raleigh, C. B., 1969, Principal stress directions from plastic flow in crystals: Geol. Soc. Am. Bull., **80**, 1231–1264.

Davis, P. M., 1983, Surface deformation associated with a dipping hydrofracture: J. Geophys. Res., **88**, 5826–5834.

Dieterich, J. H., and Carter, N. L., 1969, Stress history of folding: Am. J. Sci., **267**, 129–155.

Dieterich, J. H., and Onat, E. T., 1969, Slow, finite deformation of viscous solids: J. Geophys. Research, **74**, 2081–2088.

Evans, K. F., 1983, On the development of shallow hydraulic fractures as viewed through the surface deformation field: Part 1—Principles: J. Petr. Tech., **35**, 406–410.

Evans, K. F., and Engelder, J. T., 1986, A study of stress in Devonian Shale: Part I—3-D stress mapping using a wireline microfrac system, SPE 15609: Presented at 61st Ann. Tech. Conf. of Soc. Petr. Eng.

Federov, F. I., 1968, Theory of elastic waves in crystals: Plenum Press.

Gough, D. I., and Bell, J. S., 1982, Stress orientations from borehole wall fractures with examples from Colorado, east Texas, and northern Canada: Can. J. Earth Sci., **19**, 1358–1370.

Hickman, S. H., Zoback, M. D., and Healy, J. H., 1988, Continuation of a deep borehole stress measurement profile near the San Andreas Fault, 1. Hydraulic fracturing stress measurements at Hi Vista, Mojave Desert, California: J. Geophys. Res., **93**, 15 183–15 195.

Price, N. J., 1966, Fault and joint development in brittle and semi-brittle rock: Pergamon Press.

Shamir, G., and Zoback, M. D., 1992, A crustal stress orientation profile to 3.5 km depth near the San Andreas fault at Cajon Pass, California: J. Geophys. Res., **97**, 5059–5080.

Smith, M. B., Ren, N. K., Sorrells, G. G., and Teufel, L. W., 1986, A comprehensive fracture diagnostics experiment; Part 2—Comparison of fracture azimuth measuring procedures: Soc. Petr. Eng., Production Engineering, **1**, 423–431.

Stearns, E. W., 1968, Certain aspects of fracture in naturally deformed rocks: *in* R. E. Rieder, Ed., Nat. Sci. Found. advanced science seminar in rock mechanics, Special Report, Air Force Cambridge Research Laboratories, AD 669375I, 91–118.

Teufel, L. W., 1986, In-situ stress and natural fracture distribution at depth in the Piceance Basin, Colorado—Implications to stimulation and production of low permeability gas reservoirs: Proc. 27th U.S. Symp. on Rock Mech., 702–708.

Teufel, L. W., and Farrell, H. E., 1992, Interrelationship between in-situ stress, natural fractures, and reservoir permeability anisotropy—A case study of the Ekofisk Field, North Sea: Presented at Fractured and Jointed Rock Conf., ISRM Symp.

Warpinski, N. R., Branagan, P. T., and Wilmer, R., 1985, In-situ stress measurements at DOE's multiwell experiment site, Mesaverde Group, J. Petr. Tech., **37**, 527–536.

Warpinski, N. R., and Teufel, L. W., 1991, In-situ stress measurements at Rainier Mesa, Nevada Test Site—Influence of topography and lithology on the stress state in tuff: Int. J. Rock Mech. Min. Sci. & Geomech. Abstracts, **28**, 143–161.

Winterstein, D. F., 1990, Velocity anisotropy terminology for geophysicists: Geophysics, **55**, 1070–1088.

Winterstein, D. F., and Meadows, M. A., 1991a, Shear-wave polarizations and subsurface stress directions at Lost Hills Field: Geophysics, **56**, 1331–1348.

——— 1991b, Changes in shear-wave polarization azimuth with depth in Cymric and Railroad Gap oil fields: Geophysics, **56**, 1349–1364.

Withjack, M., and Scheiner, C., 1982, Fault patterns associated with domes—an experimental and analytical study: Am. Assoc. Geol. Bull., **66**, 302–316.

Zoback, M. D., Moos, D., and Mastin, L., 1985, Wellbore breakouts and in-situ stress: J. Geophys. Res., **90**, 5523–5530.

Zoback, M. D., Tsukahara, H., and Hickman, S., 1980, Stress measurements at depth in the vicinity of the San Andreas Fault—Implications for the magnitude of shear stress at depth: J. Geophys. Res., **85**, 6157–6173.